AEGC2019 Data to Discovery
Australasian Exploration Geoscience Conference
2-5 September 2019 • Perth, Western Australia
Incorporating the AIG, ASEG, PESA, and WABS

4D Seismic Bandwidth and Resolution Analysis for Reservoir Fluid-flow Model Applications

Rafael Souza
Centre for Energy Geoscience
The University of Western Australia School of Earth Sciences M004, 35 Stirling Hwy
Crawley, WA 6009
Australia
Rafael.medeirosdesouza@uwa.edu.au

David Lumley
Centre for Lithospheric Studies
The University of Texas at Dallas
ROC 21, 800 Wes
Richardson, Texas
USA
david.lumley@uwa.edu.au

Jeffrey Shragge
Centre for Wave Phenomena
Geophysics Department
Colarado School of Mines
924 16th Street, Golden CO
80401-1877
USA
jeffrey.shragge@uwa.edu.au

Alessandra Davolio
UNISIM – CEPETRO –UNICAMP
Cora Coralina Street, 350 CEP
13083-896, Barao Geraldo
Campinas - Brazil
davolio@cepetro.unicamp.br

Denis Schiozer
UNISIM – CEPETRO –UNICAMP
Cora Coralina Street, 350 CEP
13083-896, Barao Geraldo
Campinas - Brazil
denis@cepetro.unicamp.br

SUMMARY

Limitations on the vertical resolution in seismic data and fluid-flow models challenges the accurate interpretation of time-lapse (4D) seismic signals to identify fluid saturation changes within hydrocarbon reservoirs. Conventional streamer seismic data typically have a vertical resolution of 10-20 m at reservoir levels due to the lack of both lower and higher frequencies in the seismic spectrum, while fluid-flow simulations commonly run with significantly finer-scale vertical model grid spacings on the order of meters. Recently developed seismic acquisition methods (i.e., broadband seismic) have improved vertical seismic resolution relative to conventional acquisition by enhancing both the low- and high- frequency components. We investigate whether this improved seismic vertical resolution will result in potential benefits for fluid-flow and reservoir monitoring. We apply a synthetic 3D/4D seismic forward modelling procedure to the fine-scale fluid-flow model UNISIM-I-R, developed from observations of the Namorado field, Campos Basin, Brazil. Our procedure involves 4D seismic forward modelling, seismic amplitude map extraction, and quantitative 3D and 4D seismic amplitude analysis. Our results indicate that typical broadband seismic data can identify reservoir sands approximately 6 m thick in comparison to the 10-20 m commonly recovered in conventional seismic bandwidth. The improved seismic vertical resolution is closer to the fluid-flow model vertical grid spacing, which reduces seismic interpretation uncertainties associated with upscaling/downscaling procedures and ultimately improves the reliability of reservoir model predictions.

Key words: broadband seismic, fluid-flow model update, seismic vertical resolution.

INTRODUCTION

Time-lapse (4D) seismic has changed the way we monitor hydrocarbon reservoirs (Lumley, 1995; Lumley, 2001; Johnston, 2013). The ability of 4D seismic data to reveal fluid-flow patterns within hydrocarbon reservoirs effectively decreases the uncertainties associated with non-unique solutions provided by conventional reservoir modelling and calibration methods (e.g. fluid-flow models and history matching using production rates and pressures. Seismic data and fluid-flow models differ in many aspects with perhaps the most complex challenges involving combining information from different physical domains, across different scale lengths, and with different error sources (Lumley and Behrens, 1998). One long-standing difficulty is the vertical resolution difference between seismic data and fluid-flow models. A typical fluid-flow model has a vertical grid spacing in the order of 1-10 m, while conventional seismic data offer a vertical resolution in the order of 10-20 m. As a result of this scale-length mismatch, interpreting 3D and 4D seismic attributes in relation to properties at the reservoir scale within fluid-flow simulation grids remains challenging.

Recent advances in 3D “broadband” seismic technology enable data acquisition with broader spectral bandwidth. In general, geological models conditioned by 3D broadband seismic data are likely to be more consistent with the geological settings. Arguably, broadband seismic data reduce the uncertainty in P-wave impedance (IP) estimates by helping to constrain the addition of low-frequency information incorporated from well data or a priori models during the seismic inversion process (Souza et al., 2017).

Although significant progress has been made in analysing the improvements afforded by 3D broadband seismic data, in the context of 4D seismic applications two key questions not yet fully addressed are: (1) do 4D broadband seismic data provide time-lapse information with higher vertical resolution for fluid-flow model assessment?; if yes, (2) does this improvement lead to more accurate reservoir property estimate of uncertainties associated with upscaling/downscaling effects within the fluid-flow model grid?

To address these questions, we undertake a study involving forward modelling of the 4D seismic response to fluid-flow models as a function of seismic bandwidth.

We begin by specifying the methodology used to examine these questions, which is followed by the description of the wavelets

used in the 4D seismic modelling and analysis. We then describe the synthetic UNISIM-I-R benchmark model containing the two reservoir targets used in our numerical tests. The seismic vertical resolution of each wavelet is then analysed by quantifying the information recovered by the ΔA maps. We conclude with a discussion on the implications of these results for broadband 4D seismic attributes in workflows for estimating and/or updating reservoir properties and structural features within fluid-flow model grids, along with their potential benefits for reservoir monitoring and optimal hydrocarbon recovery.

METHOD

This section describes our methodology for verifying whether improved vertical resolution from 4D broadband seismic acquisition allows geoscientists and engineers to resolve thinner reservoir layers for fluid-flow model assessment.

4D seismic workflow

First, static and dynamic data output from a fluid-flow model are input into a petro-elastic model (PEM) to generate P-wave impedance volumes for the baseline and monitor seismic survey times, $I_P(t_0)$ and $I_P(t_1)$, respectively. The $I_P(t_0)$, $I_P(t_1)$ and derived density volumes are used to calculate zero-offset reflection coefficients at the baseline and monitor times, $RC(t_0)$ and $RC(t_1)$, respectively. Subsequently, we define the reference 4D reflection coefficients as $\Delta RC = RC(t1) - RC(t0)$. We also extract the true water saturation changes (ΔStrue) directly from the fluid-flow simulation results. Convolving $RC(t_0)$ and $RC(t_1)$ with a given wavelet generates the baseline and monitor seismic traces from which we can extract amplitude maps, $A(t_0)$ and $A(t_1)$. We then generate 4D amplitude maps by differencing the baseline and the monitor maps, $\Delta A = A(t_1) - A(t_0)$.

We identify a thin and thick reservoir target for our study and extract a ΔA map of the largest trough (maximum negative peak amplitude) within a given time window. The reservoir targets and time windows are defined on a case-by-case basis; therefore, we defer providing these details until discussing each particular case below. A similar procedure can be applied to extract maps from the ΔRC volume. Note that there is no wavelet effect on the ΔRC estimates because they are extracted directly from the $I_P(t_0)$ and $I_P(t_1)$ volumes output from the PEM. Thus, we may use ΔRC as a reference because it directly indicates the true locations of lithological interfaces. The ΔRC values are commonly smoothed until they exhibit the same resolution of the seismic attributes. However, we avoid this here to achieve our goal of comparing data with the full frequency band (i.e., “infinite resolution” maps) with those with various more restricted seismic resolutions.

In this study, we use three different wavelets that cover a wide range of commonly observed seismic data bandwidths (see Table 1). We represent more conventional seismic spectra using two band-passed zero-phase impulses denoted C1 and C2, while our broadband seismic spectra is modelled as a band-passed delta -function denoted BB. The pulse width and sampling interval of all wavelets are 200 ms and 1 ms, respectively. While exhibiting a slightly broader spectrum than C1, the C2 wavelet also has more pronounced sidelobes when compared with the BB wavelet, which ultimately affect the wavelet width and corresponding seismic vertical resolution. We also apply two unrealistically high (for exploration seismic) band-passed wavelets U1 and U2 that allow us to explore improved seismic vertical resolution resulting from the additional frequency bandwidth.

The wavelets C1, C2 and BB are input to the simulation-to-seismic workflow described above to extract ΔA maps as a function of seismic bandwidth. Thus, the question at hand is how does each wavelet affect the capability of their respective ΔA maps to accurately estimate the location of the difference of contrasts between any given porous media (e.g. ΔRC)? We examine this question below in the context of the UNISIM-I-R benchmark model.

We model UNISIM-I-R seismic amplitude response at the times of the baseline (t0 = 0 days) and monitor (t1 = 4, 068 days) seismic surveys. We first extract static (e.g. porosity, net-to-gross) and dynamic (e.g. pressure, water saturation) properties used as input into a PEM estimating IP and IS volumes. We use net-to-gross estimates to infer shale percentage at each grid cell. The pressure constant between seismic surveys to help isolate the effects of ΔSW on ΔA estimates.

We assume an average P-wave velocity (Vp=2.5 km/s) within all the simulation cells while converting the fluid-flow model from depth to two-way travel time (TWT) for both the baseline and monitor surveys. We calculate RC from the computed IP volumes using the normal-incidence plane-wave approximation (Telford et al., 1990), and subsequently convolve these estimates with the different seismic wavelets to generate the synthetic 3D seismic trace data volumes. We apply the same modelling procedure to generate the monitor survey data. Having modelled the two seismic surveys, we extract seismic amplitude maps ΔA.

RESULTS

Figure 1 shows Areas 1 and 2 and the arbitrary line (AL). This region contains three horizontal producers (PROD023, PROD024 and PROD025), two horizontal injectors (INJ007 and INJ010), and is isolated from the rest of the reservoir by the known sealing fault FB. INJ007 and INJ010 are completed in Layers 63 and 68 and commence water injection after approximately 2000 and 2200 days of production, respectively. The injection strategy focuses on sustaining reservoir pressure and thereby supporting the oil production rate. PROD023A is completed in Layer 63 and starts producing water after 3167 days, while PROD024A is completed at Layer 8 and starts producing water after approximately 2600 days. Finally, PROD025, completed at Layer 19, starts producing water after approximately 2500 days.

This observed water breakthrough indicates that the water injected within deeper layers moves up dip eventually reaching the three producing wells, thereby revealing the presence of more localised high vertical permeability trends.

Figures 2a-c present 4D seismic data changes ΔAC1, ΔAC2 and ΔABB along the AL seismic section, respectively. The broadband ΔABB cross section resolves the thinner sand in Area 2 while traditional wavelet cross sections again fail to do so. In Area 1, the conventional and broadband wavelets provide similar qualitative information as both identify the reservoir sand.

Overall, we observe qualitatively that the ΔABB map (in Figure 3d) retrieves more information of the reference ΔRC map than either of the ΔAC1 and ΔAC2 maps (Figures 3b-c, respectively). The ΔAC1 and ΔAC2 maps (Figures 3b-c) are

poorly correlated with the ΔRC map as they fail to retrieve most of the ΔRC map information.

We first extract maps of ΔA and the true water saturation changes (ΔStrue) within the polygons in Figure 4. The left column of Figure 5 superimposes the crossplots of ΔRC versus ΔStrue in Area 1 with those of the C1, C2 and BB counterparts, respectively. We then superimpose the histogram of each ΔA and ΔRC for each wavelet type (right column of Figure 5). Overall, each wavelet captures the general decreasing ΔRC trend due to the increase in ΔStrue. For Area 2, Figures 6a, c and e superimpose the crossplots of ΔRC, True ΔAC1, ΔAC2 and ΔABB against ΔS, respectively. While Figures 6b, d and f highlight that the ΔAC1, ΔAC2 and ΔABB overestimate the histograms of the ΔRC, Figures 6b, d and f show that the respective wavelets underestimate the ΔRC histogram.
In general, the histograms in both areas are poorly correlated with the reflection coefficient changes. This suggests that finite resolution affects the modelled seismic amplitudes and require further investigation.

ANALYSIS

Our results lead us to the following three discussion topics: (1) what causes the mismatch of the amplitude and reflection coefficient histograms in Areas 1 and 2; (2) what is the influence of the additional broadband frequencies relative to conventional wavelets on the 4D fluid- flow seismic modelling?; and (3) what are the practical implications using broadband 4D seismic attribute estimates for fluid-flow model assessment and calibration? We discuss each topic below.

Vertical resolution and seismic amplitude analysis

To further investigate why $_{\Delta AC1}$, ΔAC2 and ΔABB maps fail to accurately estimate ΔRC, we extract the reflection coefficients calculated from the PEM from the baseline survey along two pseudo-wells located in Areas 1 and 2. Table 2 shows that the number of RC per wavelength ranges from two to eight and therefore falling in the medium-frequency regime, with several (>2 and <100) discontinuities per seismic wavelength. The wavefield experiences sub-wavelength layer-related phenomena such as reflection, transmission, multiples, and mode conversion. These layer-related processes cause the wavefield to decrease in amplitude (attenuation by scattering) by a frequency/wavelength dependent amount. While higher frequencies in the propagating wavefield attenuate much faster than lower frequencies, interbed multiples can reinforce the downgoing wavefield and thus partially offset this effect through constructive and destructive interference (O'Doherty and Anstey, 1971). Overall, quantifying the seismic amplitude response due to layered media effects can be achieved by comparing full-waveform modelling results (e.g. through finite difference solutions) to those generated by infinite frequency ray-tracing and convolution modelling results (Liu and Schmitt, 2006). However, this task that is beyond the scope of our proof-of-concept study. Table 2 indicates that our results represent a scenario falling within the medium-frequency resolution regime. This means that the "apparent" ΔAC1, ΔAC2 and ΔABB measure the upscaled RC instead of the fine-scale RC, thus accounting for the differences between the histograms of the band-limited and infinite bandwidth fine-scale reflection coefficients observed in Figures 5 and 6.

In principle, we could obtain one reflector per wavelength by increasing the frequency of the convolved wavelet. The resulting histograms of the seismic amplitude changes would then be more consistent with the fine-scale RC in Figures 5 and 6. To test this supposition, we apply the unrealistically high band-passed wavelets U1 and U2 (see Table 1) to estimate the seismic amplitude change maps ΔAU1 and ΔAU2, respectively. After applying the methodology described above we superimpose ΔAU1 and ΔAU2 and ΔRC histograms for Areas 1 and 2 (Figures 7a-d). Note that these histograms match and therefore confirming our supposition that a broader spectra would capture the ΔRC distribution.

In both Areas 1 and 2, ΔAU1 and ΔAU2 histograms are more similar to the ΔRC distribution than ΔABB, respectively. As the bandwidth asymptotes to infinity, the histograms of seismic amplitudes and RC values would move toward a near-perfect match. This test illustrates that reservoir models with sub-wavelength layer thicknesses may produce complex and non-intuitive seismic amplitude responses.

Impact of broadband 4D seismic attributes on fluid-flow model procedures

These results lead to two key questions regarding the use of broadband 4D seismic data in fluid-flow model workflows: (1) what are the benefits of the additional lower and higher frequencies of the seismic data?; and (2) how do these additional frequencies affect 3D/4D synthetic seismic modelling of the dynamic response of fluid-flow models?

Overall, the BB wavelet results in a sharper image that provides additional details about finely layered reservoir structure. The reduced sidelobes provided by the lower frequency content decrease interference between top and base of sand reflections. For instance, Figure 2 shows stronger sidelobe effects caused by the C1 and C2 wavelets compared to those resulting from BB wavelet images.

Our results show that in thin sand units, such as the one analysed in Area 2, the higher frequency content of broadband seismic data improves both vertical and lateral resolution in comparison to conventional acquisition. In our case, the increased number of reflection coefficients per wavelength affects the resolution regime and therefore the reflection amplitudes (if observed) start to change in manners particularly hard to characterize. Amplitudes are no longer the same as the high-frequency RC values (i.e., those calculated from the Zoeppritz equations). Rather, they become significantly more complex due to the presence of more than 1 or 2 reflectors per wavelength. Consequently, these effects increase the uncertainties associated with quantitative applications of seismic amplitudes, such as ΔSW estimates derived from ΔA maps or seismic inversion results.

Overall, our results show that while broadband seismic data provides useful additional information relative to conventional acquisition, there will still be seismic resolution issues for thin reservoir layers (relative to the broadband seismic wavelength) that can produce complex and non-intuitive seismic amplitude responses. Thus, it is important to analyse the seismic resolution regime on a case-by-case basis.

CONCLUSIONS

Our quantitative analysis and study confirms that broadband seismic data offer improved vertical seismic resolution, and retrieve more spatial information than conventional acquisition. Our examples show that the maps of amplitude changes derived from broadband seismic data for the UNISIM-I-R reservoir

model retrieve 30% more horizontal reflection coefficient information than conventional seismic data in the thick reservoir target (Area 2). The enhanced low- and high-frequency content of the broadband wavelet reduces sidelobes and improves seismic vertical resolution, thereby improving the overall quality of the 4D fluid-flow seismic amplitude data. Ultimately, these improvements should lead to more ac- curate seismically derived attributes for use in seismic history matching workflows. We also observe that the resolution regime changes reflection amplitudes in complex ways that are difficult to interpret without full wavefield modeling and analysis. In summary, our results should help to motivate the development of qualitative and quantitative applications of 4D broadband seismic data for calibration and assessment of fluid-flow models.

Table 1. Frequency corners of the C1, C2, BB, U1 and U2 wavelets.

Wavelets	Low-cut (Hz)	Low-pass (Hz)	High-pass (Hz)	High-cut (Hz)
C_1	0	20	40	60
C_2	0	10	60	80
BB	0	5	100	150
U_1	0	5	100	200
U_2	0	5	150	250

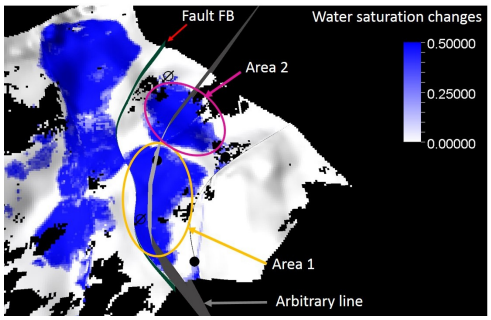

Figure 1. The ΔSW distribution within Layer 65 of the UNISIM-I-R fluid-flow model that we use to define interpretation Areas 1 and 2 and the arbitrary line (AL).

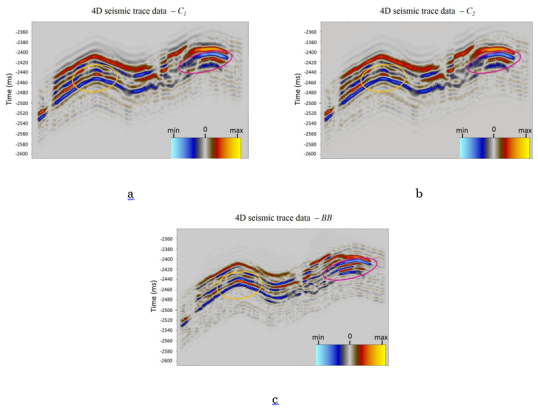

Figure 2. Seismic cross sections in time along the arbitrary line AL (see Figure 4) of: (a) ΔAC1; (b) ΔAC1; and (c) ΔABB. Areas 1 and 2 are highlighted in yellow and pink, respectively.

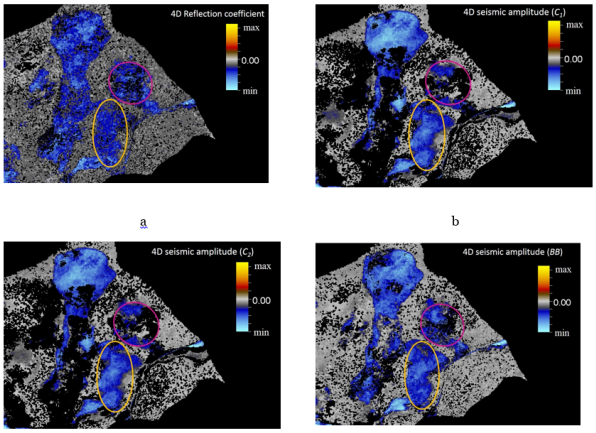

Figure 3. Maps of the largest trough within 10 ms below the horizon in Figure 9 of: (a) ΔRC; (b) ΔAC1; and (c) ΔAC2; and (d) ΔABB. Areas 1 and 2 are highlighted by the yellow and pink ovals, respectively.

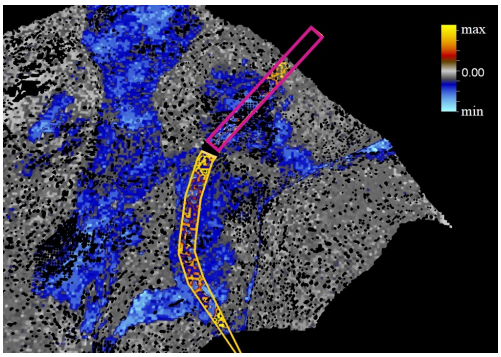

Figure 4. ΔRC map superimposed with Area 1 and Area 2 polygons along AL (in yellow and pink, respectively) used for cross-plotting ΔA attributes against ΔSW.

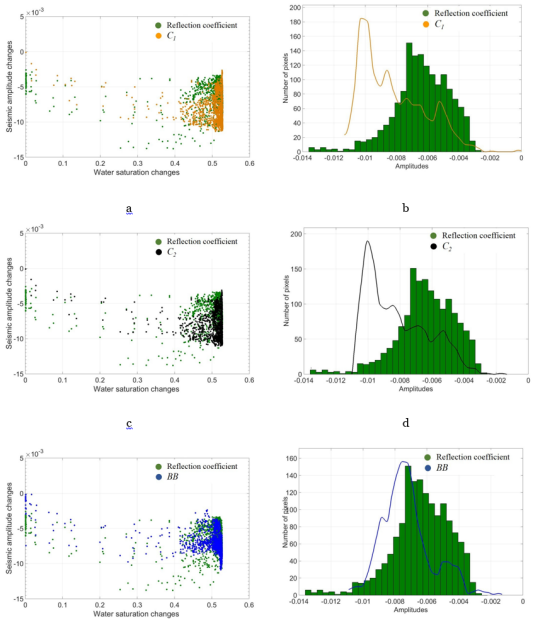

Figure 5. Comparison of Area 1 ΔRC cross-plot against ΔSW with ΔA maps (left column) and their histograms (right column) derived from wavelets: (a-b) C1; (c-d) C2; and (e-f) BB.

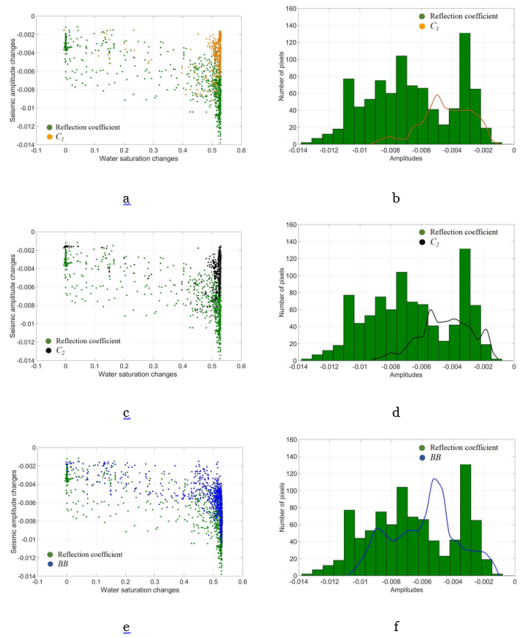

Figure 6. Comparison of Area 2 ΔRC cross-plot against ΔSW with ΔA maps (left column) and their histograms (right column) derived from: (a-b) C1; (c-d) C2; and (e-f) BB seismic data, respectively.

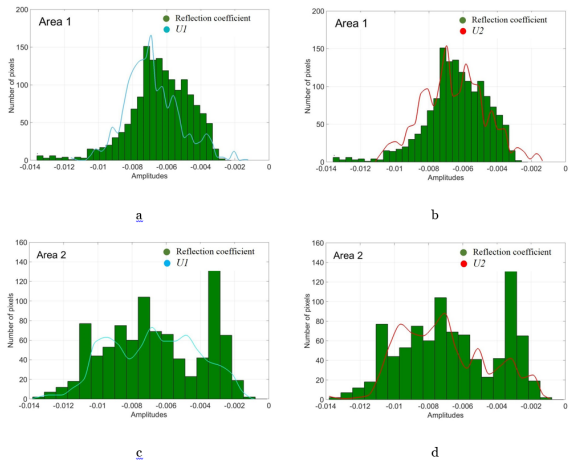

Figure 7. Superimposition of the ΔRC and ΔAU1 and ΔAU2 histograms in Areas 1 (a-b) and 2 (c-d), respectively. Note that in comparison to ΔAC1, ΔAC2 and ΔABB, the histograms of the ΔAU1 and ΔAU2 are more similar to ΔRC distribution.

REFERENCES

Avansi, G., and D. Schiozer, 2015, UNISIM-I: Synthetic Model for Reservoir Development and Management Applications: International Journal of Modeling and Simulation for the Petroleum Industry, 9, 21–30.

Johnston, D, 2013, Practical Applications of Time-lapse Seismic Data (2013 DISC): Society of Exploration Geophysicists.

Liner, C. L., 2012, Elements of seismic dispersion: A somewhat practical guide to frequency- dependent phenomena: Society of Exploration Geophysicists.

Lumley, D., 1995, Seismic Time-Lapse Monitoring of Subsurface Fluid Flow: PhD thesis, Stanford University.

———, 2001, Time lapse seismic reservoir monitoring: Geophysics, 66(1), 50–53.

Lumley, D., and R. Behrens, 1998, Practical Issues of 4D Seismic Reservoir Monitoring: What an Engineer Needs to Know: SPE Reservoir Evalution & Engineering, 1(6), 528–538.

O'Doherty and Anstey, 1971, Reflections on amplitudes: Geophysical Prospecting, 19, 430– 458.

Souza, R., D. Lumley, and J. Shragge, 2017, Estimation of reservoir fluid saturation from seismic data: amplitude analysis and impedance inversion as a function of noise: Journal of Geophysics and Engineering, 14(1), 51–68.

ten Kroode, F., S. Bergler, C. Corsten, J. W. de Maag, F. Strijbos, and H. Tijhof, 2013, Broadband seismic data - The importance of low frequencies: Geophysics, 78(2), WA3–WA14.